Characterizing Density for Low Density, Ultra-Cold Plasmas

by Measuring the Free Expansion Rate of Coulomb Explosion

Nathan Rock

A senior thesis submitted to the faculty of
Brigham Young University
in partial fulfillment of the requirements for the degree of

Bachelor of Science

Scott D Bergeson, Advisor

Department of Physics and Astronomy

Brigham Young University

June 2012

ABSTRACT

Characterizing Density for Low Density, Ultra-Cold Plasmas
by Measuring the Free Expansion Rate of Coulomb Explosion

Nathan Rock
Department of Physics and Astronomy
Bachelor of Science

We develop a diagnostic to measure the density of ultra-cold, neutral plasmas by measuring the free expansion rate during Coulomb explosion. We expect this method to be accurate at very low densities, where current methods are ineffective. We derive a model for the expansion of low density plasmas which gives plasma radius as a function of of time and density. Plasma radius can be measured with high precision even at very low densities, giving this method good resolution where optical methods lose sensitivity. We attempt to confirm this model experimentally, and discover that stray electric fields deflect the plasma causing the our method to underestimate density.

Keywords: ultra-cold, neutral plasmas, UCP, Coulomb explosion, plasma, expansion rate, plasma density, strong coupling parameter, strongly coupled plasmas, density diagnostic, plasma radius

ACKNOWLEDGMENTS

I would like to thank my advisor, Dr. Scott Bergeson, for the immense amount of work he has spent training me. I am at a loss to explain his patience and generosity, as he hardly seems to get a return on the investment. I hope one day I can be as positive, hardworking and compassionate as he is.

I would also like to thank Dr. Van-Heule and Dr. Ware for their tireless work reading drafts, commenting and encouraging in Physics 416. Without their help I'm not sure this thesis ever would have been completed.

Contents

Chapter 1

Introduction

1.1 Motivations and Project Goal

In physics, a plasma refers to a collection of atoms which have been partially or completely ionized. Plasmas exist in everyday life and throughout the universe on different scales. In astronomy astral bodies like stars and nebulae ionize gas at several million Kelvin. These plasmas occur at temperatures at or above room temperature and predominantly at extremely high temperatures. Our research deals with plasmas on the far other end of the temperature scale. We produce ultracold ($\sim 30mK$) plasmas in vacuum. Our goal is to create strongly coupled plasmas. In strongly coupled plasmas the Coulomb interaction between the particles dominates over thermal energy; That is, the strong coupling parameter, $\Gamma \equiv \frac{e^2}{4\pi\varepsilon_0 a_{WS}} \frac{1}{k_B T}$ is greater than or equal to one. For $\Gamma > 1$ the plasma begins to exhibit liquid behavior and for $\Gamma > 20$ the plasma "freezes" and begins to exhibit a crystalline structure [1].

Researchers studying ultra cold plasmas in this setting regularly need a reliable measure of density. When measuring the strong coupling parameter the potential energy relates to the Wigner-Seitz radius (a_{WS}) which in turn relates to density. Density is a key factor in mapping the veloc-

ity distribution of expanding plasmas [2] to determine the ion temperature of the plasma and in studying the three body recombination rate [3], both of which are essential elements in achieving stronger coupling in plasmas. Despite this, there are currently few published methods to accurately measure density. Those that do exist lose sensitivity at low densities. [2]

We seek to develop a reliable method to measure densities at these low densities. Our method relies on measuring the free expansion rate of the plasma during Coulomb explosion. This can be measured with high accuracy at low density.

1.2 Overview of Current Diagnostic Methods

We are aware of four published methods for measuring plasma density: optical absorption imaging of the plasma ions, measurement of the transmission of a "probe" laser beam through the atomic sample before and after ionization, RF heating of the electrons, and direct measurement of the RF absorption of the plasma.

Optical absorption imaging of plasma can be done after ionization. Atoms are captured in an atomic trap and ionized using resonant laser light. Using a CCD camera, one takes absorption images of the plasma. The ions absorb and scatter light out of the path of CCD creating a dark spot on the camera representing the atoms. Analysis of the absorption image yields the density of the plasma. This process was first demonstrated by Killian et al in 2004 [4]

This method shows the full density distribution in the plane parallel to the camera lens. It also allows one to see how that distribution evolves over time by varying the time lapsed from plasma creation to camera exposure. However, at very low densities the difference in absorption may be extremely small and this method loses sensitivity.

A probe beam can be used to measure the percentage of ionization of the experimenter's atomic trap. This method is similar to optical absorption imaging described above, but it uses a narrowly

collimated beam of resonant light to measure only a small portion of the trap. Absorption of the probe beam before and after ionization is measured using a photo-multiplier tube (PMT). This device responds to light by producing current which is proportional to the intensity of the light shown on its surface. The change in the PMT signal is directly related to the density of the plasma.(see section 2.3.3)

The use of a PMT instead of a CCD camera provides a more easily quantifiable method and increases the sensitivity of the measurement. However, the researcher cannot be certain whether they are measuring the peak density of the trap, or the less dense edge or local abberation, and again the method loses sensitivity at low densities.

In the method of RF heating of electrons [5], plasma is ionized and a radio frequency (RF) field is applied to the atoms, imparting thermal energy to the electrons. The plasma expands due to the mutual repulsion of the atoms, and the density decreases. An ion detector picks up electrons freed from the plasma. Upon ionization the ions create a potential well, trapping the ionized electrons in shells near the plasma. The plasma partially absorbs the RF signal, heating the nearby electrons and allowing them to escape towards the detector. The plasma absorbs the RF power primarily when the electron plasma frequency (ω_p) matches the applied RF frequency. When this condition is met, electrons are ejected from the plasma and measured. Since the plasma frequency depends on density, this method can be used to measure the density as a function of time.

Rolston and Twedt have reported direct measurement of the RF absorption of a plasma [6]. This method is similar to the method of RF heating of electrons. An RF field causes the plasma to oscillate in time. Here however, no ion detector is used. Instead, the oscillating plasma induces a current in a nearby wire. The RF signal also induces a current. By mixing the signal from the RF field with that of the wire they are able to isolate the signal from the plasma oscillations. Using a theoretical model in which plasma frequency depends on plasma density, they are able to use the plasma oscillations to measure plasma density.

This method does not rely on fluorescence measurements or an ion detector. However, it relies on signals which are much smaller than that of the RF signal it is subtracted from. These signals are done at very high frequency. As such it has a high signal to noise ratio. They report needing a minimum of 150 averaged signals to properly resolve the plasma oscillations from the background noise. This difficulty becomes larger and larger at lower densities, where the oscillations are smaller and produce less moving charge.

1.3 Free Expansion Method

Because the methods described above rely on optical devices such as a photo-multiplier tube (PMT), they become ineffective at low densities where only a few photons are absorbed. The absorption of the atoms is difficult to measure against the background noise. Our method side steps this issue. We create a singly-ionized plasma from calcium atoms and accelerate it towards an ion detector as shown in figure 1.1. As the plasma passes through the detector, it produces a signal like that in figure 1.2. This signal corresponds to the density distribution of the plasma in the direction that the plasma is moving.

We create the plasma from a Gaussian atomic trap so the signals have a clear rising and falling edge (see Fig 1.2). We refer to the half-height between the rising and falling edge as the radius of the plasma. In a perfectly Gaussian plasma, the radius is the full width half max of the density distribution.

The plasma expands as the positively charged ions repel each other. A more dense plasma will have more ions in close proximity and will thus expand faster. At a given time after ionization, a denser plasma will have a wider profile than a less dense plasma. Thus, by measuring the profile of the ion detector signal at a given time after ionization we can extract the density.

In section 2.1 we derive a simple model which relates initial density, radius and expansion

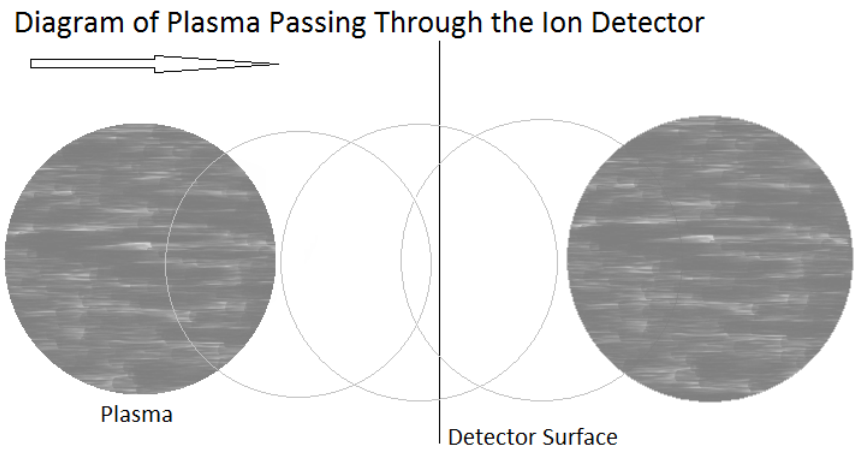

Figure 1.1 Diagram of plasma moving through the detector

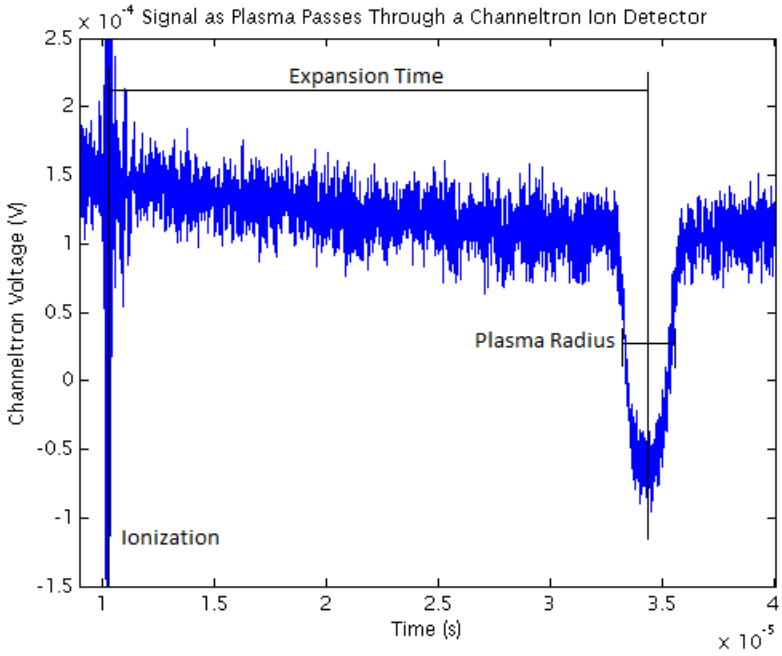

Figure 1.2 Raw ion detector signal. The spike at the left signals ionization. The detector registers flat line until the plasma reaches it. It dips down as the plasma passes through it and returns to flat line as the trailing edge passes through.

time. In section 2.2 we describe our laboratory set up and our attempts to confirm this model, linking density and radius at a fixed expansion time. To do so, we ionized calcium in vacuum and accelerated it towards a detector. We vary the density to trace out the density vs radius curve at

fixed expansion time. Chapter 3 gives the analysis of the data and its comparison to the model.

As we progressed through our experiment, we discovered that while the method has high resolution in the required variables, and thus should accurately predict the plasma density, it is sensitive to inhomogeneities in the electric fields in the chamber. These fields significantly alter the signal by the time it gets to the detector. As such, in the end our experiment failed to yield satisfactory results. We are currently looking at ways to improve the experiment to overcome this difficulty. In section 3.4 we describe an alternative laboratory set up which we are currently implementing. In this set up the electric fields are carefully controlled to eliminate distortion of the plasma by stray fields.

Chapter 2

Methodology

2.1 Development of Model

2.1.1 Description and Assumptions

Our model gives the plasma radius as a function of expansion time and density. We model the plasma as a uniform sphere of positive charge. The plasma is assumed to expand self-similarly as the positively charged ions repel each other, keeping the same overall shape and distribution, but decreasing in density. We assume that all atoms in the sphere have been ionized and that all electrons have been removed from vicinity of the plasma and do not effect the evolution of the plasma in time.

When modeling this as a differential equation, we track a "test charge" on the outermost edge of the plasma. For a sphere of N charges distributed uniformly the electric field is,

$$\oint \bar{E} \cdot d\bar{a} = 4\pi r^2 E = \frac{Ne}{\varepsilon_0} \Rightarrow E = \frac{Ne}{4\pi\varepsilon_0 r^2} \tag{2.1}$$

where e is the fundamental charge ($1.602 \times 10^{19} C$) and r is the plasma radius. Thus, the repulsive force on the test charge is,

$$F = m\ddot{r} = \frac{Ne^2}{4\pi\varepsilon_0 r^2} \Rightarrow \ddot{r} = \frac{Ne^2}{4\pi\varepsilon_0 m r^2} \tag{2.2}$$

where m is the mass of the ions and ε_0 is the permittivity of free space.

2.1.2 Solving the ODE

Solving this ODE proves more complicated than one might expect, as it is non-linear and second order. In the end we actually get expansion time as a function of current radius and density and we have to solve the function numerically from there. The derivation is as follows.

Note that,

$$\frac{\partial}{\partial t}\left(\dot{r}^2\right) = 2\dot{r}\ddot{r} \tag{2.3}$$

and,

$$\frac{\partial}{\partial t}\left(\frac{-1}{r}\right) = \frac{\dot{r}}{r^2} \tag{2.4}$$

so,

$$\ddot{r} = \frac{Ne^2}{4\pi\varepsilon_0 m r^2} \tag{2.5}$$

$$\Rightarrow \quad 2\dot{r}\ddot{r} = \frac{\partial}{\partial t}\left(\dot{r}^2\right) = \frac{Ne^2}{2\pi\varepsilon_0 m}\frac{\dot{r}}{r^2} = \frac{Ne^2}{2\pi\varepsilon_0 m}\frac{\partial}{\partial t}\left(\frac{-1}{r}\right) \tag{2.6}$$

$$\Rightarrow \quad \dot{r}^2 = -\frac{Ne^2}{2\pi\varepsilon_0 m}\frac{1}{r} + C_1. \tag{2.7}$$

When the plasma is first created the radial velocity is zero so,

$$\dot{r}(0)^2 = 0 = -\frac{Ne^2}{2\pi\varepsilon_0 m}\frac{1}{r_0} + C_1 \Rightarrow C_1 = \frac{Ne^2}{2\pi\varepsilon_0 m}\frac{1}{r_0} \tag{2.8}$$

where r_0 is the initial radius of the plasma.

We would like to have our final answer in terms of density rather than particle number. The density of a uniform sphere of particles is simply,

$$n = \frac{N}{\frac{4}{3}\pi r^3} \Rightarrow N = \frac{4}{3}\pi n r^3 \tag{2.9}$$

where lower case n is density. However our density is not constant in time. We seek the initial density corresponding to initial radius (r_0) rather than the radius as a function of time ($r(t)$). That is,

$$N = \frac{4}{3}\pi n_0 r_0^3 \tag{2.10}$$

We introduce n and r_0 and find that we can now resize our variables in favor of the dimensionless quantity $\tilde{r} \equiv \frac{r(t)}{r_0}$.

$$\dot{r}^2 = \frac{Ne^2}{2\pi\varepsilon_0 m}\left(\frac{1}{r_0} - \frac{1}{r}\right) = \frac{\frac{4}{3}\pi n_0 e^2}{2\pi\varepsilon_0 m}\left(\frac{r_0^3}{r_0} - \frac{r_0^3}{r}\right) \tag{2.11}$$

$$\Rightarrow \frac{\dot{r}^2}{r_0^2} = \dot{\tilde{r}}^2 = \frac{2ne^2}{3\varepsilon_0 m}\left(1 - \frac{r_0}{r}\right) = \frac{2n_0 e^2}{3\varepsilon_0 m}\left(1 - \frac{1}{\tilde{r}}\right) \tag{2.12}$$

Solving this equation in Maple yields the following equation giving time of expansion as a function of radius and density.

$$t = \frac{3}{8}\sqrt{\frac{6\varepsilon_0 m}{n_0 e^2}}\left(2\sqrt{\tilde{r}(\tilde{r}-1)} + ln(2) + ln[2\tilde{r} - 1 + 2\sqrt{\tilde{r}(\tilde{r}-1)}]\right) + C_2 \tag{2.13}$$

At $t = 0$ the resized radius equals 1 (the radius is the initial radius). Thus,

$$0 = \frac{3}{8}\sqrt{\frac{6\varepsilon_0 m}{n_0 e^2}}\left(2\sqrt{1*(0)} + ln(2) + ln[2*1 - 1 + 2\sqrt{1*(0)}]\right) + C_2 \tag{2.14}$$

$$\Rightarrow C_2 = -\frac{1}{4e}\sqrt{\frac{6\varepsilon_0 m}{n}} ln(2) \tag{2.15}$$

Our model gives the following relation between expansion time, radius and density

$$t = \frac{1}{4e}\sqrt{\frac{6\varepsilon_0 m}{n}}\left(2\sqrt{\tilde{r}(\tilde{r}-1)} + ln[2\tilde{r} - 1 + 2\sqrt{\tilde{r}(\tilde{r}-1)}]\right) \tag{2.16}$$

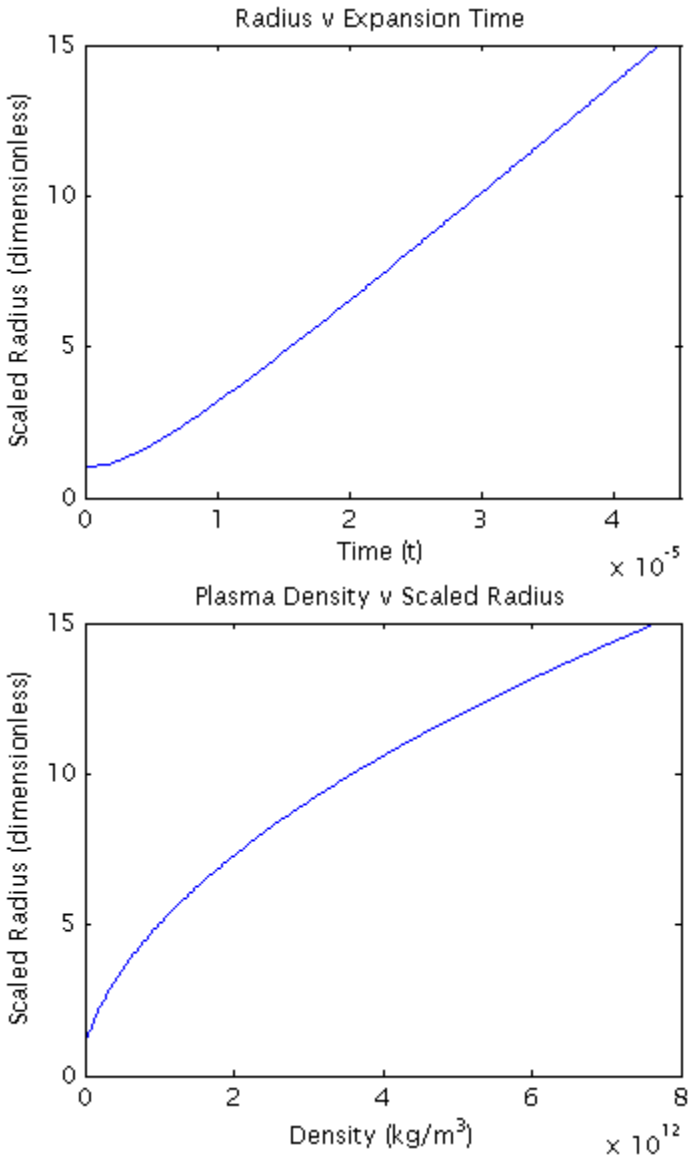

Figure 2.1 Graph of the free expansion model using singly ionized calcium: holding density constant and varying flight time (top) and holding flight time constant and varying density (bottom)

A graph of this equation for a given initial density (Fig 2.1) shows the behavior one would expect (flipping the axes to appease our physics intuition). As the ions move away from one another, the Coulomb repulsion they exert on one another falls to effectively zero and the plasma expands at a nearly constant velocity. Here, the ion's inertia is responsible for most of the expansion, and

radial velocity is nearly constant. Figure 2.1 is a graph of the model. The first figure holds initial density constant and shows how the scaled radius changes with time. The second figure holds flight time constant and shows how the scaled radius changes with density.

2.2 Laboratory Setup

2.2.1 Overview

To confirm our model for free expansion we ionize atoms, creating plasma, and accurately measure the plasma radius as it passes through a detector. We apply an external electric field to extract the plasma and accelerate it towards the detector. This field was fixed during our experiment giving us a fixed time of flight (expansion time). We vary the density of the plasmas to trace out the radius vs. density curve for the model.

Using a probe beam like that described in section 1.2 we are able to get an independent measure of density. By overlaying plots of density vs scaled radius of these data points with a plot of the model for those densities, we can determine how well the method predicts density.

We took data from April 19, 2011 to April 27, 2011, leaving out the weekend of April 23 and 24. Each day we took from 21 to 34 data sets. Each data set consists of two signals - one from a photo multiplier tube (PMT) and one from a Channeltron ion detector. These signals are averaged over 32 sequential ionizations under the same conditions. The signals are taken in each of four states corresponding to the the open or shut states of shutters in front of the probe beam and the beam of atomic trap (see sec 2.2.3). As such each data set consists of four signals for the PMT and four signals for the Channeltron. We collected a total of 187 data sets.

2.2.2 Capturing Atoms for Ionization in a Magneto-Optical Trap

We create our plasma in high vacuum ($1 \times 10^{-8} Torr$) by capturing and cooling calcium atoms in a magneto-optical trap (MOT). A MOT uses Zeeman splitting to cool atoms and confine them to a very small area. The technique was first demonstrated by Raab and Chu in 1987 [7].

Our source for trapping is an atomic beam of calcium atoms. We heat calcium atoms to 580°C in a reservoir on one side of our chamber. They travel through a $10mm$ long tube, $1mm$ in diameter, and form an effuse beam. Some of these atoms pass through the MOT.

We coil wire above and below the center of the vacuum chamber and run a current clockwise above the chamber and counterclockwise below, creating a magnetic field in the chamber. The field is zero at the center of the chamber. As one travels radially outward the magnitude of the field grows linearly but the direction of the field is positive in one direction and negative in the opposite direction. We shine laser light at $423nm$ through this zero point on three axes in in both a positive and negative direction. This light is slightly detuned from the resonance transition of the atoms.

Valence electrons in calcium have a total orbital quantum number of $j = 0$. At a certain distance from the center of the field (the MOT radius) Zeeman shifting of the $m = +1$ and $m = -1$ levels brings the resonance transition down to that of the MOT laser light propagating in one direction as shown in Fig 2.3. As atoms travel in the positive direction they reach the MOT radius where the $m = -1$ level is shifted into resonance with the $\sigma-$ beam. Radiation pressure from the beam pushes the atoms back towards the center of MOT. As atoms reach the MOT radius traveling in the negative direction they radiate under the influence of the $\sigma+$ beam and are again pushed back into the MOT.

This technique allows us to cool the neutral atoms to $\approx 3mK$ prior to ionization. Figure 2.2 shows the layout of the MOT. Figure 2.3 is a diagram showing the MOT's effect when atoms move outside the zero field region.

To maximize the efficiency of our MOT we add two other laser beams - a "slower beam" and

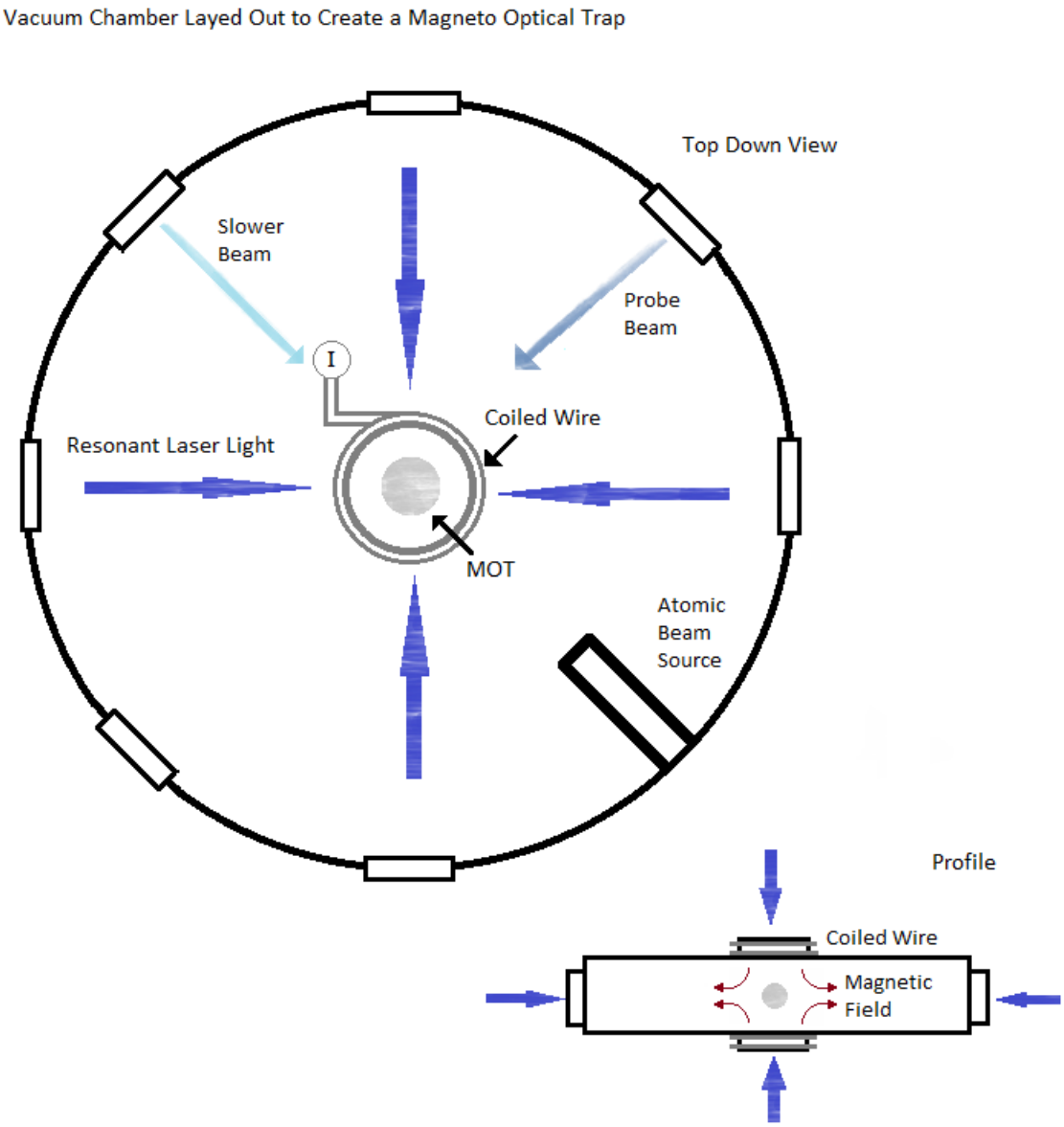

Figure 2.2 Layout of the vacuum chamber to create a Magneto Optical Trap. The coiled wire produces a magnetic field which is zero only at the center. Atoms in the zero field region feel no effect. Atoms outside the zero field region experience Zeeman splitting. Laser light resonant with the Zeeman shifted energy levels cause the atom to radiate energy and fall back into the zero field region.

a "repump" beam. The slower beam is detuned so that it is just below the resonance frequency of the atoms. We place it head on with the atomic beam. The Doppler shift causes the highest energy

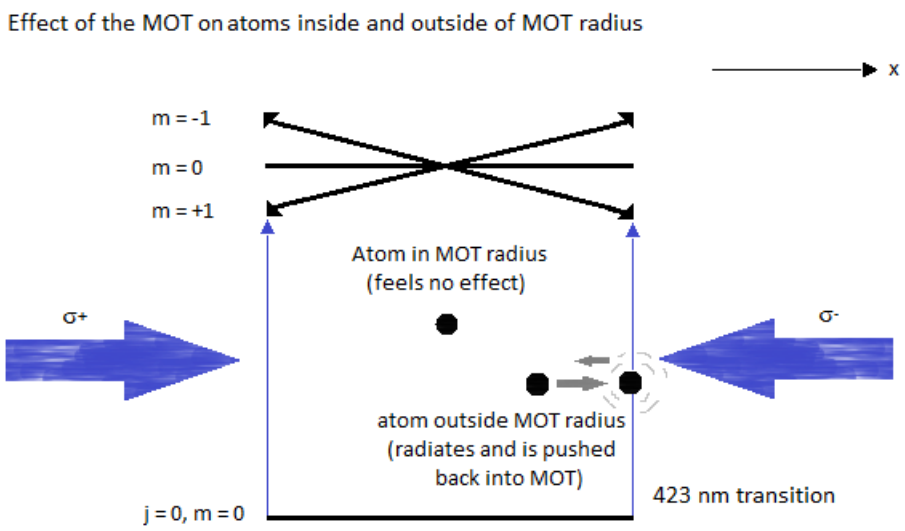

Figure 2.3 Atoms in the zero field region are not affected by the MOT beam. As the atoms move out of the zero-field region, the MOT beams cause them to radiate energy outward.

atoms in the atomic beam to perceive the beam as being on resonance. They radiate energy and slow down. Without this beam, a high percentage of the atoms in the atomic beam would be too energetic to be trapped. The beam slows many of the atoms so they are able to be trapped in the MOT.. Adjusting the orientation of the slower beam often produces an increase in absorption of 10 to 20 percent in optical absorption imaging measurements.

We implement the repump beam to circumvent a difficulty in Calcium's energy structure. The MOT beams are tuned to $423nm$ causing a transition from the ground state to the $4s4p^1P_1$ level. Between the ground state and this level lies a metastable state. As the MOT causes atoms to radiate, a percentage of them fall into this "dark state." Here, they do not feel the effect of the MOT beams. The atoms trickle away and the maximum absorption of the MOT is decreased by typically 10 to 15 percent. The repump beam is tuned to the transition between this dark state and the excited state. Atom's which fall into the dark state get repumped back into the excited state and eventually fall back to ground level. The repump beam has a wavelength of $672nm$.

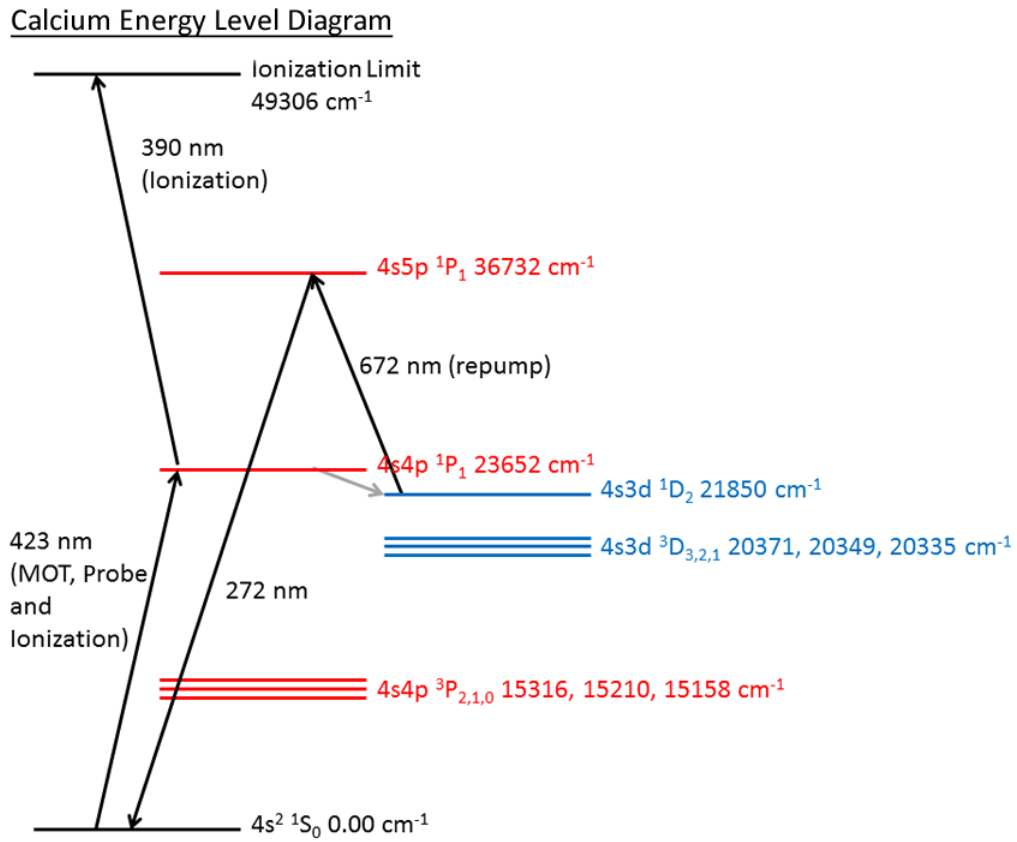

Figure 2.4 Calcium energy level diagram. Pertinent transitions labeled with their application.

2.2.3 Measuring Density via Optical Absorption of the Probe Beam

We take optical absorption measurements at the beginning and end of every day of data collection. This gives us a good idea of the size and uniformity of the MOT (and thus the plasma), and it allows us to see how the density of our MOT has changed throughout the day.

To take optical absorption images we take a piece off of the MOT beam using a beam splitter. We refer to this as the probe beam for its use later in the set up. An Acousto-Optic Modulator (AOM) returns this beam to the unshifted resonance frequency of the atoms, causing the atoms to absorb its light. We use a spherical lens to spread the beam out over the entire cavity. Using LabVIEW, we take a series of pictures using cameras to extract the optical absorption of the un-

Table 2.1 Summary of Lasers

Summary of Lasers		
Name	λ (nm)	Description
MOT Beam	423	*Captures and cools neutral atoms*
Slower Beam	detuned from 423	*Cools high velocity atoms in atomic beam to increase efficiency of MOT*
Repump Beam	672	*Excites atoms which have fallen into the metastable dark state. Increases MOT efficiency*
Probe Beam	423	*Used for optical absorption measurements before and during data collection*
Ionizing Beam	423, 390	*Ionizes atoms to create plasma*

ionized MOT. We use two cameras at different angles to be sure the MOT is in fact spherical.

Fluorescence in the chamber can come from the MOT, the probe beam, or the background of the MOT. To get an image of the MOT alone automatic shutters are positioned to cut off the MOT beam and probe beam. We take four photos - one with both shutters open, one with both shut, one with the MOT shutter closed and the probe shutter open and one with the probe shutter closed and the MOT shutter open. We run 30 cycles in quick succession and average the results. A Matlab script then extracts the absorption of the MOT alone. In section 2.3 Analysis I describe our method for these computations in more detail.

Figure 2.5 shows a typical optical absorption measurement. The dark center in the absorption image and the bright center in the emission image are the result of the MOT. The darkest spots in the absorption image are the densest areas of the MOT while the areas which are only slightly darker than the background are less dense. In aligning the MOT beams, we attempt to make the density fall off uniformly, giving the MOT a Gaussian shape.

These measurements give us a good idea of the density and density distribution of the MOT

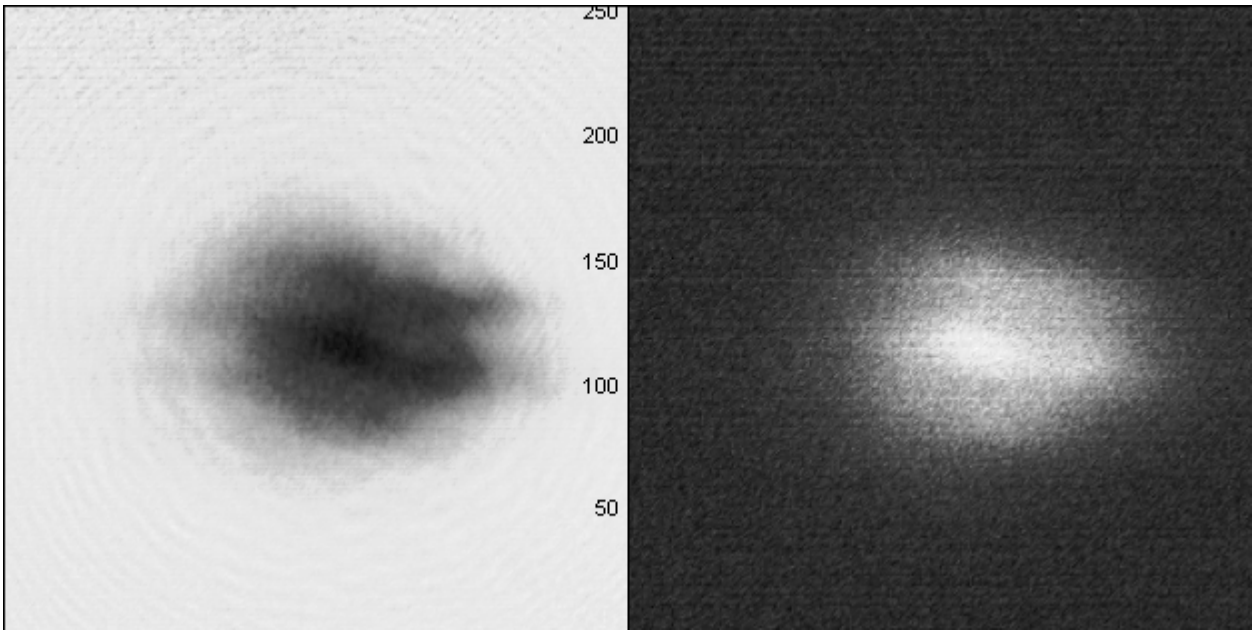

Figure 2.5 Optical Absorption Measurement data taken Apr 20 2011
Absorption (L) Emission (R)

prior to ionization, but their relationship to the density of the plasma is unclear without more information. We leave the probe beam in the chamber during ionization, but we cannot do optical absorption imaging during the data collection process. Optical absorption measurements take more than a minute, while our data is on the order of microseconds, and the ionizing beam would completely saturate the cameras in any case. Thus, during ionization we remove the spherical lens and keep the beam narrowly collimated. The beam passes through a small cross section of the entire MOT and is picked up by a photomultiplier tube (PMT). Upon ionization, An electric field extracts the plasma from the region of the MOT. When the plasma is formed, the transmission of the beam jumps. The density of the plasma can be determined from this difference in transmission.

Figure 2.6 shows a typical signal from the PMT. Note the sudden drop signaling ionization. The difference between transmission before and after ionization represents the density of the extracted plasma.

These measurements lose sensitivity at all but our highest density data sets. On their own they

cannot give a reliable measure of density. For all other data points, we integrate the ion signal to get a relative measure of the density. The absolute measure from from the probe beam serves as an anchor for these relative measurements, allowing us to give them real values.

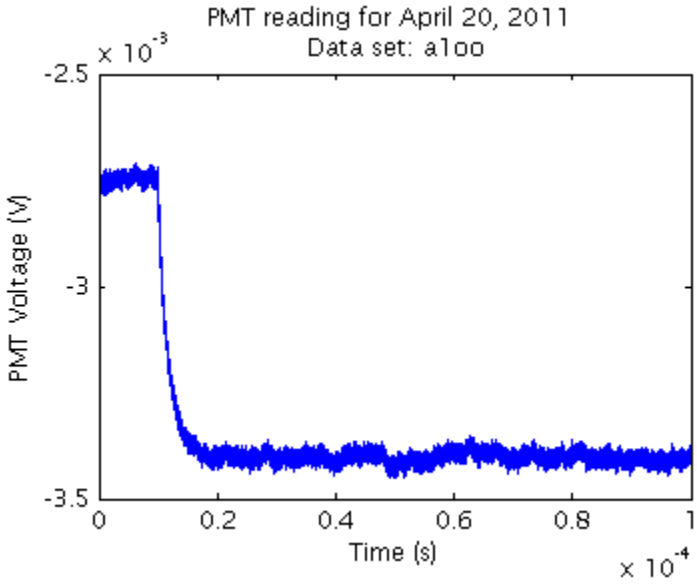

Figure 2.6 PMT reading for data taken Apr 20 2011
Data set a1 in the open-open position. Note the sudden drop in signal around $10\mu s$ as the ionized plasma leaves the detector

2.2.4 Ionization, Data Collection and Tracing the Curve

We ionize the atoms using a two stage ionization. A pulsed laser excites the atoms at $423nm$. Another pulsed laser then ionizes them at $390nm$. After ionization, the electric field causes the positively charged ions begin to move towards a Channeltron ion detector.

Table 2.1 summarizes the lasers involved, their wavelengths and a brief description of their purpose in the project.

Our goal is to trace out the radius vs density curve at fixed time of flight. We use multiple methods to vary density. Our first method is to use neutral density filters in the path of the ionizing beam. We begin at plasma densities which give good resolution in the probe beam and work down

until the signal width ceases to decrease. As we move down, we block the repump beam and slower beam. This decreases the density of the MOT and thus the density of the plasma.

For more finely tuned measurements, we adjust a shutter in front of the atomic beam. The atomic beam source can be shut off several milliseconds before the ionizing beam arrives, allowing the number of atoms in the MOT depth to decrease. In practice we preferred this method, since it allowed a wide range of finely tuned variations in density.

At each density we produce a data set consisting of four ion detector signals generated by the moving plasma and four PMT signals generated by transmission of the probe beam through the MOT. We use LabVIEW to average 32 ionizations under the same conditions in each of these states.

2.2.5 Varying the Ion Detector Sensitivity and Determining r_0

The ion detector has a variable sensitivity which can easily be burned out if the signal jumps too high. During each day of data collection, we begin at high density and lower ion detector sensitivity (usually 1150 V). As we lower the density the ion signal decreases in depth. When the signal becomes hard to resolve we raise the sensitivity on the ion detector (usually to 1350 V). The difference in gain here is unclear and we need to get a good measure of the relationship between the size of plasmas at high and low ion detector sensitivity for our relative density measurements. Accordingly we take two data sets at low sensitivity, and before we alter the density we take two more data sets at high sensitivity. In Chapter 3 I explain our method for correlating the high and low sensitivity measurements.

The final element in our setup is determining the initial radius of the plasma. The model gives time as a function of resized radius. Each of the radii determined from the ion signal must be divided by the initial radius of the plasma which is unknown. To determine the scaled radius we note that at very low densities the plasma hardly expands at all. Thus, when measuring radii of

plasmas we decrease density until the radius hardly changes at all from one density to another. We take this as the initial radius for all higher density measurements.

2.3 Analysis Process

2.3.1 Interpretation of Signal and Analysis Overview

This set up yields two signals - one from the probe beam as it hits the PMT and one from the Channeltron ion detector.

As the MOT is ionized, transmission jumps and the signal on the PMT drops. The difference between transmission before and after indicates the density of the plasma. On each day of data collection we could only resolve the drop in signal for our densest two to four data sets. For the rest, we observe that the integrated ion signal represents the total number of ions passing through the detector. Thus the integrated ion signal is proportional to plasma density. We integrate the ion signal for each data set and draw a line of best fit to give us the relative density between them. The densest probe beam signals, for which we can resolve the drop in transmission, serve as an absolute reference, linking this relative scale to absolute density.

The ion detector measures the ionized plasma passing through it. It registers a flat line when no ions are present. As the front end of the moving plasma passes through the detector the signal drops and as the back end of the signal passes through the detector the plasma returns to flat line (see Fig 1.2). The full width half max of this signal dip reflects of the radius of the plasma.

The expansion time of the plasma is equivalent to the time of flight of the plasma from creation until it hits the detector. The time of plasma creation is clearly marked by the sudden drop in signal on the PMT. To get the total time of flight we take the midpoint between the leading and trailing edge of the ion signal signal minus the dropping time in the PMT signal (See Figure 2.7).

Manipulation of these signals maps out the radius vs density curve of the plasma for fixed

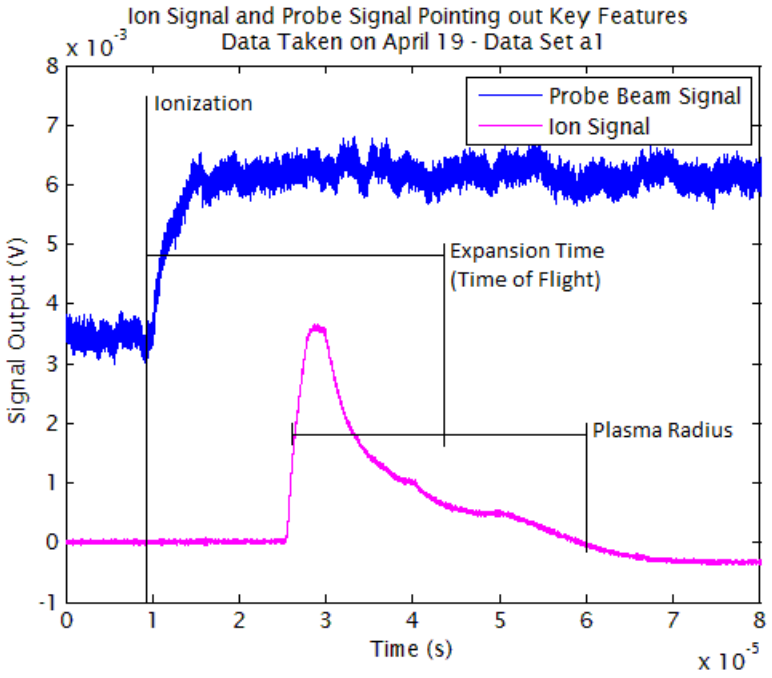

Figure 2.7 Probe beam signal and ion signal with key features indicated after processing to isolate signal from the MOT only. Data taken on April 19, 2011. Data set $a1$. The probe beam signal has been scaled down by a factor of 30 and shifted down so the key features of each signal may be seen in the same shot.

expansion time. We compare this to our model.

2.3.2 Determining Radius and Time of Flight

To determine the value of our model, we need the flight time and radius of each signal. As we looked at our signals we discovered that we would need to measure each full width half max signal and the time of flight of each signal by hand.

We expected our signals to be roughly Gaussian. Optical absorption measurements show that the MOT is densest in the middle and that density falls off radially towards zero with only small localized pockets of high density (see Figure 2.5). If the plasma structure reflects that of the MOT, as we would assume, the moving plasma passing through the ion detector should cause the signal to rise slowly until the dense middle of the plasma and then drop gradually as the back end of the

plasma thins out giving it a Gaussian shape. Instead, our largest signals look like Figure 2.8, with a tall peak at early times, an exponential-like drop off and a smaller peak at trailing end. Deciding what constitutes the radius of the plasma requires the user to specify the radius manually.

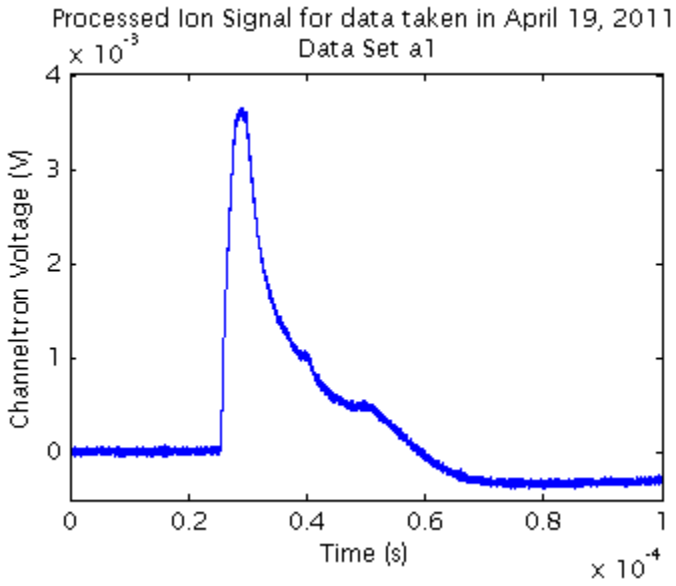

Figure 2.8 Signal for a high density plasma after processing to isolate the plasma signal from the background. Data taken on April 19, 2011. Data set a1

To extract these signals we write a Matlab script which allows the user to manually specify the width and flight time of each signal. Since even the largest signals like that in figure 2.8 have a sharp leading and trailing edge, we mark the radius of the plasma by the first and last distinct edge of the signal. Any dips or troughs between the first and last peaks we attribute to non uniformities in density.

The script loads each data point in the open-open (open MOT beam shutter, open probe beam shutter), close-open (close MOT shutter, open probe beam shutter), open-close, and close-close states. During our experiment we ionize atoms from both the MOT and the dark signal from the background of the chamber. For our data to best reflect our model we must remove this ionization of stray atoms not caught in the MOT. Also, our ion detector displays the plasma as a drop in signal and for aesthetic purposes it would be nice to see the signal "right side up." For each temporal point

in a data set we use the following equation to extract the MOT ionization from the raw ion signal:

$$ion = (-oo + oc - co + cc)/2 \tag{2.17}$$

Here, oo refers to the open-open signal, oc refers to open probe closed MOT, etc. The open open signal includes the MOT signal and dark signal. The close probe beam open MOT signal does as well. The open probe beam closed MOT signal and the closed probe beam closed MOT signal register only the dark signal.

$$\begin{aligned} ion &= (-oo + oc - co + cc)/2 \\ &= (-(MOT + DarkSignal) + DarkSignal - (MOT + DarkSignal) + DarkSignal)/2 \\ &= -MOT \end{aligned} \tag{2.18}$$

This manipulation gives us the signal from the MOT only and averages the signal. Figure 2.9 shows each of the signals (oo,oc,co,cc) and their physical meaning. Figure 2.10 is the processed signal, giving only an average of the MOT signal alone.

The Matlab script averages every 30 points to smooth noise. It then prompts the user to pick two points for the baseline and two points to measure to mark the signal width and one for the center of the plasma. It saves the signal width and the center point.

The flight time (corresponding to the mid point of the signal) turns out to be almost the same for each data point. This is what we would expect. Each ion in the plasma is the same mass and is subject to nearly the same external electric field and will thus experience the same acceleration over the same distance.

To get the scaled radius from this full width half max measurement, we use the very smallest data points. As explained in Section 2.2.5, at the lowest densities, the plasma hardly expands at

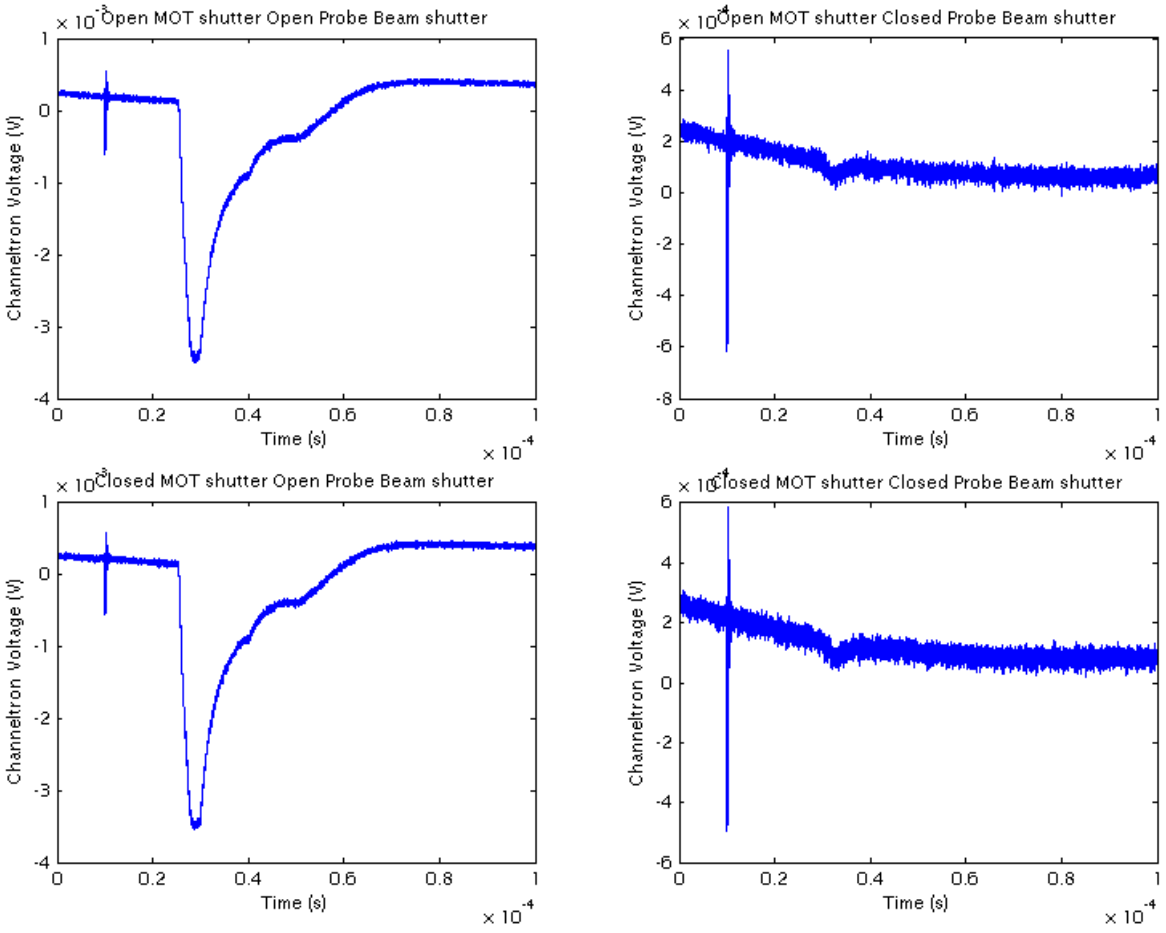

Figure 2.9 Ion signal in each state for data taken on April 19, 2011. Data set a1

all. As such we define the initial radius, r_0, as

$$r_0 = v_f \Delta t_0 = v_f \Delta t_{min} \tag{2.19}$$

Where Δt_min is the full width half max of the ion signal for the least dense plasmas. We note that the model gives expansion time as a function of scaled radius $\tilde{r} = r/r_0$.

$$\tilde{r} = \frac{r}{r_0} = \frac{v_f \Delta t}{v_f \Delta t_{min}} = \frac{\Delta t}{\Delta t_0} \tag{2.20}$$

Thus, to get the scaled radius we need only divide the full width half max of a signal by the smallest full width half max signal for that day.

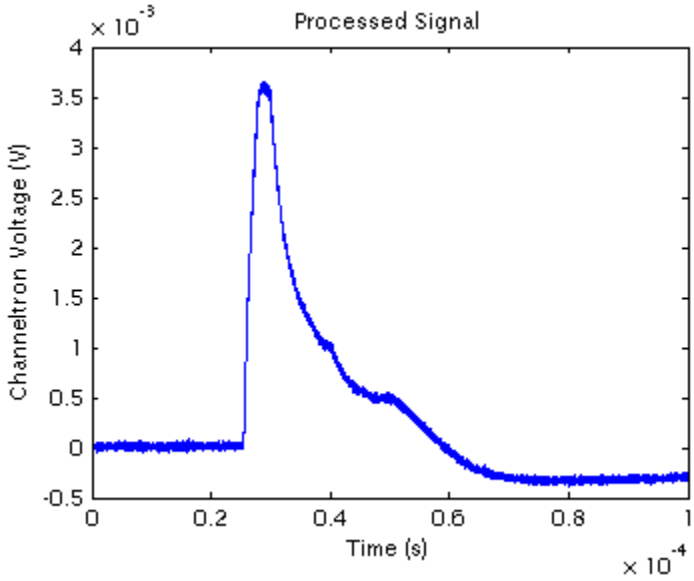

Figure 2.10 Processed ion signal for the same data.

2.3.3 Measuring Density and Fitting the Data

The probe beam measures density via optical absorption, giving us an independent measurement. Unfortunately, In only the densest two or three data sets each day can we resolve the jump in probe beam transmission. For the rest we integrate the signal under the curve of the manipulated signal using a simple Riemann sum. This integration produces a relative measure of density, while the probe beam measurements give absolute density to use as a anchor point.

To get a density measurement from the probe beam we first manipulate the signals from the four shutter states to isolate the transmission of the MOT from that of the background.

$$probe = \frac{oo - co}{oc - cc} = \frac{(Fluorescence + Absorption + DarkSignal) - (Fluorescence + DarkSignal)}{(Fluorescence + DarkSignal) - DarkSignal} = Absorption \quad (2.$$

We then average the probe signal before the ionization and those after the average of the signal after the drop. For a Gaussian plasma of density $n(\bar{r})$

$$n(\bar{r}) = n_0 exp\left(-\frac{r^2}{2r_0^2}\right) \tag{2.22}$$

Where n_0 is peak density and r_0 is the rms width of the plasma. For the transmission T of a beam oriented in the z direction

$$\begin{aligned} T(x,y,z) &= T_0(x,y)exp\left(-\int n(x,y,z)\sigma dz\right) && (2.23)\\ \Rightarrow\ -ln\left(\frac{T(x,y,z)}{T_0}\right) &= \int_0^{z_f} n(x,y,z)\sigma dz = \sigma n_0 \int_0^{z_f} exp\left(-z^2/2r_0^2\right) dz && (2.24) \end{aligned}$$

For peak density we let $x = 0, y = 0, z_f = \infty$

$$\begin{aligned} -ln\left(\frac{T(x,y,z)}{T_0}\right) &= \int_0^{z_f} n(x,y,z)\sigma dz = \sigma n_0 \int_0^{\infty} exp\left(-z^2/2r_0^2\right) dz \\ &= \sigma n_0 \sqrt{2\pi r_0^2} && (2.25)\\ \Rightarrow\ n_0 &= -ln\left(\frac{T(x,y,z)}{T_0}\right)\frac{1}{\sigma\sqrt{2\pi r_0^2}}. && (2.26)\\ & && (2.27) \end{aligned}$$

The plasma density is equal to the change in density due to the ionizating beam. We therefore write

$$ln\left(\frac{T_2}{T_0}\right) - ln\left(\frac{T_1}{T_0}\right) = ln\left(\frac{T_2}{T_1}\right) \tag{2.28}$$

so

$$n_0 = -ln\left(\frac{T_2}{T_1}\right)\frac{1}{\sigma\sqrt{2\pi r_0^2}} \tag{2.29}$$

This produces an absolute measure of density for a few high density points. We use these densities as a reference point and plot their density as a function of the integrated ion signal they produce. We perform a linear fit of these points. The slope of this line gives us a factor of integrated signal to real density which we then apply to those data points for which the probe beam gives no meaningful signal.

The ion detector has an adjustable sensitivity given in volts. When this sensitivity is raised, signals increase in depth though their width is fixed by the speed of the moving plasma.

During data collection we start at a density where the probe beam produces a well defined drop and go down until the signal is barely visible. We then perform two measurements at the same density and ion detector sensitivity and two measurements at the same density but higher sensitivity, in order to calibrate the change in sensitivity.

During analysis we average the two data points on either side of the adjustment. We plot integrated signal vs real density, and note that there is a distinct jump at the point where we adjust the ion detector sensitivity, causing the data sets to lie on top of one another. For the high density points, when the sensitivity is low the factor we obtain from the probe beam is accurate. For the points measured after the adjustment it is inaccurate. We apply a correction factor to the low density points, guessing and checking until they line up with the high density points in the expected way. Figure 2.11 shows real density plotted as a function of integrated signal without the adjustment factor for data taken on April 25, 2011 and Figure 2.12 shows the same data with the adjustment factor.

We now plot plasma radius as a function of initial density and overlay a plot of the model, with the density points chosen to match those of our data set.

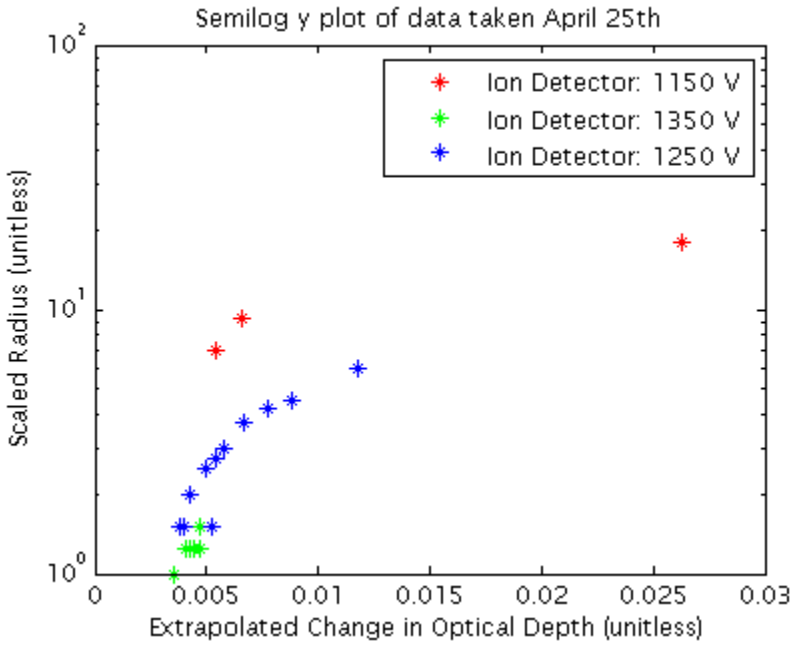

Figure 2.11 scaled radius vs change in optical depth of the probe beam as extrapolated from integrated ion signal. Each color represents a different ion detector sensitivity. Note how points with the same ion detector sensitivity each other, but they do line up not relative to those taken at a different ion detector sensitivity. Data taken on April 25, 2011.

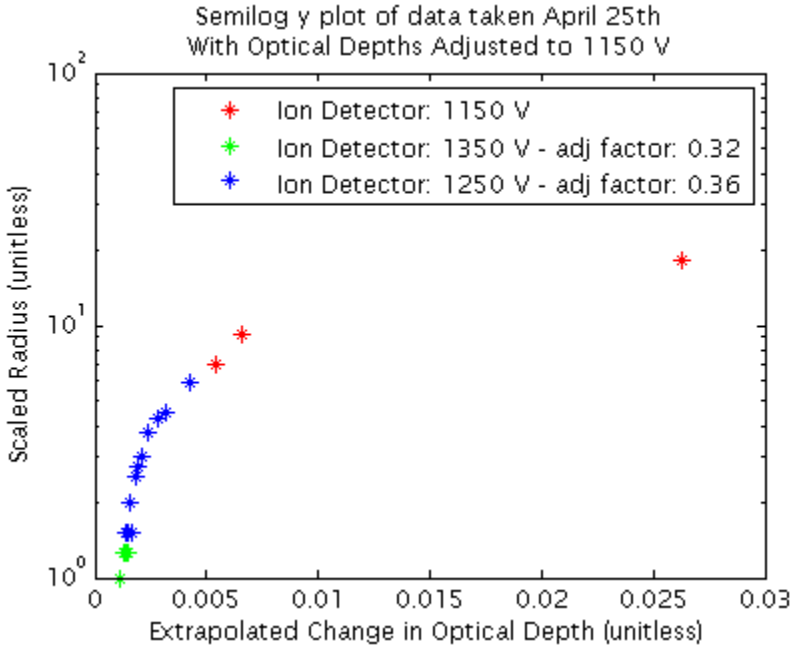

Figure 2.12 The same data, but adjusted to the optical depth of the highest density points (for which the jump in transmission resolves well). The data sets taken with the ion detector set at 1350V and 1250V have been multiplied by the factor given in the legend.

Chapter 3

Analysis and Conclusion

3.1 Results

Figure 3.1 shows scaled radius vs density for our data and the model for all five days of data collection. The model is shown as a continuous line and data points are shown as circles. Clearly the free expansion model underestimates density by a large factor. Figure 3.2 shows the same data but with the model multiplied by a factor of 20.4. From this we see that the model has more or less the correct shape, but it underestimates the average numerical value by a considerable margin.

3.2 Sources of Error

Our data is thus far unsatisfactory. The shape however is encouraging. It implies that it is not the model which is the problem, but our experimental set up.

In trying to identify the source of this discrepancy we attempt to model the electric field which extracts the plasma. Using the model of a cylinder with a voltage across its width we saw that the field generated is parabolic. As such, the final velocity of the plasma is strongly determined by its initial starting position in the field. Changes in initial position of the plasma center, which

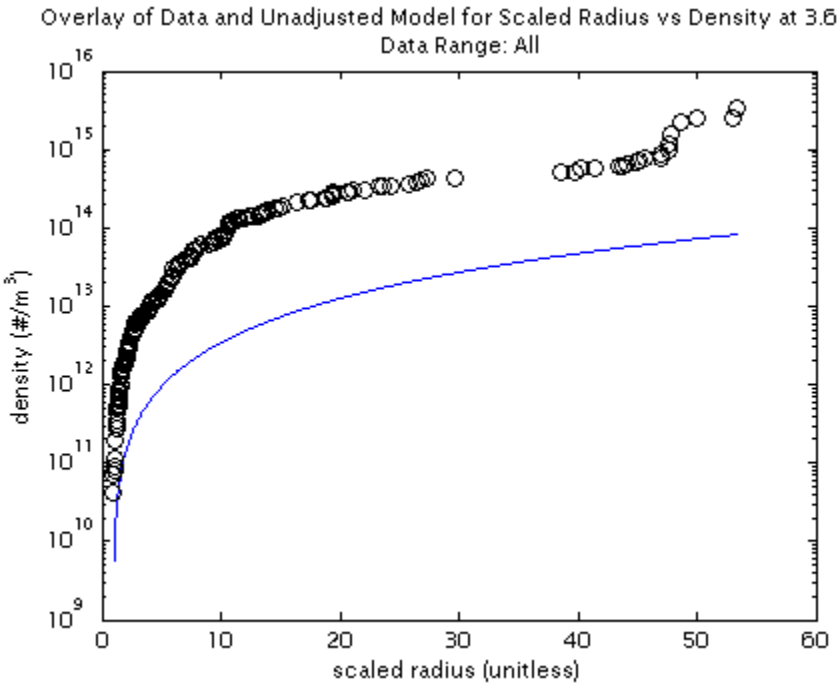

Figure 3.1 Semilog plot of scaled radius vs density at $36\mu s$ of all collected data points (circles) and the free expansion model (line)

are much smaller than the radius of the plasma are still significant enough to dominate in the final plasma radius. We believe this accounts for the factor of 20.4 difference.

Inhomogeneities in the extraction field may also play a role. The MOT is positioned close to the atomic beam. We use an electronically controlled shutter on the beam to cut off the flow between shots. This shutter produces an unmeasured field, which may be distorting the plasma early on.

3.3 Conclusion

The free expansion model derived in section 2.1 overestimates density by a factor of 20.4. This is too high to be of any use as a method for determining density. However, the shape of the curve and the model fit well. This suggests that the model is viable and that the discrepancy is the result of

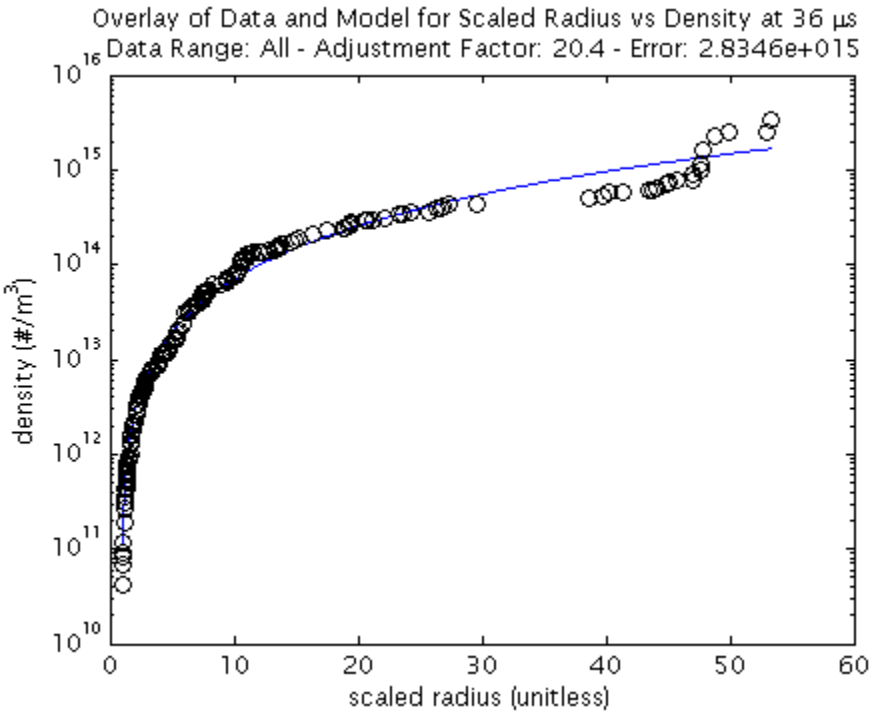

Figure 3.2 Semilog plot of scaled radius vs density at $36\mu s$ of all collected data points (circles) and the free expansion model (line), with the model adjusted by a factor of 20.4 and the summed error

our experimental set up.

We believe inhomogeneities in the field used to extract the plasma cause the model to underestimate density, but we expect that with more controlled fields it would predict density accurately.

3.4 Proposed Alternative Setup

We are currently developing an alternative set up which we hope will fix the problems discussed. In this set up we first move the atomic beam back away from the MOT. This will reduce the distortion of the extraction field by the shutter. The shutter will be positioned behind a grounded aperture to the far side of the plasma.

We set up the MOT between two stainless steel mesh grids. One is hooked up to an adjustable voltage. The other is grounded and attached to a long grounded steel tube. The plasma is accelerated in the controlled field between these grids and then allowed to expand in the field free region in the long grounded tube before it is picked up on the ion detector.

By confining the extraction field to a these plates we ensure that the extraction is linear and does not depend strongly on where in the field the plasma was created. We also shield the region from stray electric fields like those of the atomic beam shutter.

We hope to publish the results of this new set up once it has been implemented.

Appendix A

Attempts to Control For Stray Electric Fields and Results

A.1 Follow Up on Alternative Laboratory Set-Up

The data presented above was taken during April of 2011. The following winter we altered the set up of the experiment to better control the electric fields. As described in section 3.3, we believed that stray electric fields distorted the plasma, causing the expansion model to underestimate the density of the plasma.

We redesigned the set up of the vacuum system and the charge plates and took new data. We took data during March, April and May of 2012, pausing between each day of data collection to perform analysis and make minor alterations to the laboratory set up to improve the reliability of our new data.

After several months of data collection it became clear that our new data did not mirror the basic shape of the expansion model derived in section 2.1. We now believe that on a basic level the expansion model does not accurately describe the dynamics of the plasma, and that a new model

of the expansion will be necessary if the project is to continue.

A.2 Altering the Vacuum System to Control for Stray Electric Fields

A.2.1 Original Vacuum System Design

The original lay out of the vacuum chamber consisted of MOT beams coming in on three axes, a probe beam and a repump beam. The vacuum chamber consists of a $12in$ diameter cylindrical chamber with windows along its rectangular face. The ion detector sits within this chamber. A $1in$ diameter wire mesh grid sits in front of the detector and another grid sits on the far side of the MOT from it. An adjustable power supply produces a voltage drop across these grids, creating the extraction voltage which accelerates the plasma towards the detector. The grids are separated by about $4in$. The atomic beam oven sits very close to the MOT to maximize atom capture. A remote controlled shutter sits in front of the atomic beam, within a few inches of the MOT.

I have identified three sources of stray electric field in the chamber. Plastic and nylon parts in the chamber may build up charge producing a small electric field. Wires attached to the grids and atomic beam shutter produce small electric and magnetic fields. The atomic beam shutter turns on and off each cycle, producing electric fields. The fields from to atomic beam shutter probably contribute most to stray electric fields, but we attempt to reduce all contributions in our new set-up.

The distorted fields we see in the April 2011 data may also be the result of inhomogeneities in the extraction field itself. The two grids in the extraction field are placed far apart, an unequal distance from the MOT. When performing a simple model of the fields we observe that the field increases exponentially as one moves towards the ion detector. The new set up produces a linear fields between the plates.

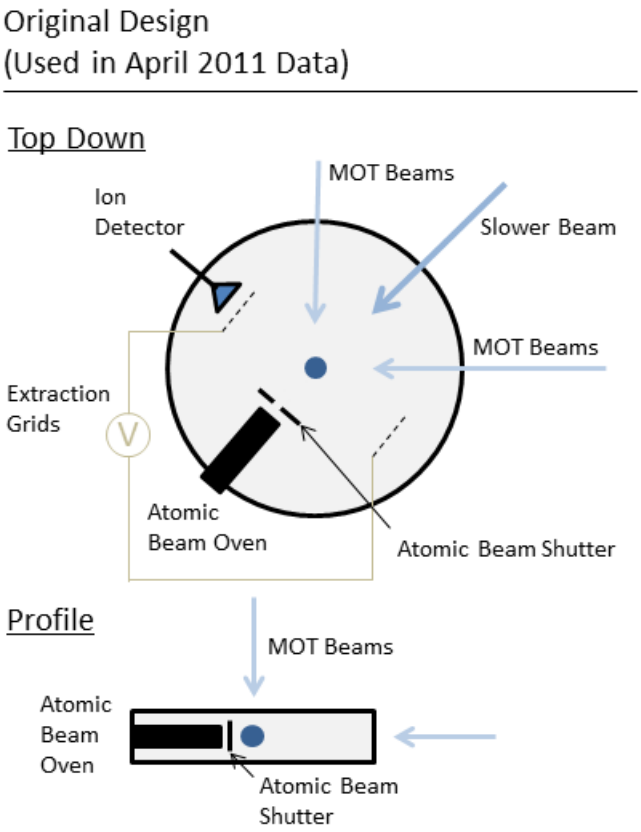

Figure A.1 Original set-up of the experiment. Note that the extraction grids are spaced very far apart and the atomic beam over and remote shutter are very close to the plasma.

A.2.2 New Vacuum System Design

In our new design, the plasma is extracted upwards along the major axis of the chamber. Two $1.125in$ diameter grids are placed above and below the plasma. They are separated by $62mm$ with the MOT centered between them. These grids are wider than those used in the original set-up, and closer together. This wider, narrower field region should shield the plasma from any small fields outside of the extraction region.

Adjustable power supplies are hooked up to each of these grids with the chamber as ground. Thus, we can vary both the strength of the extraction field and its offset from the ground of the chamber.

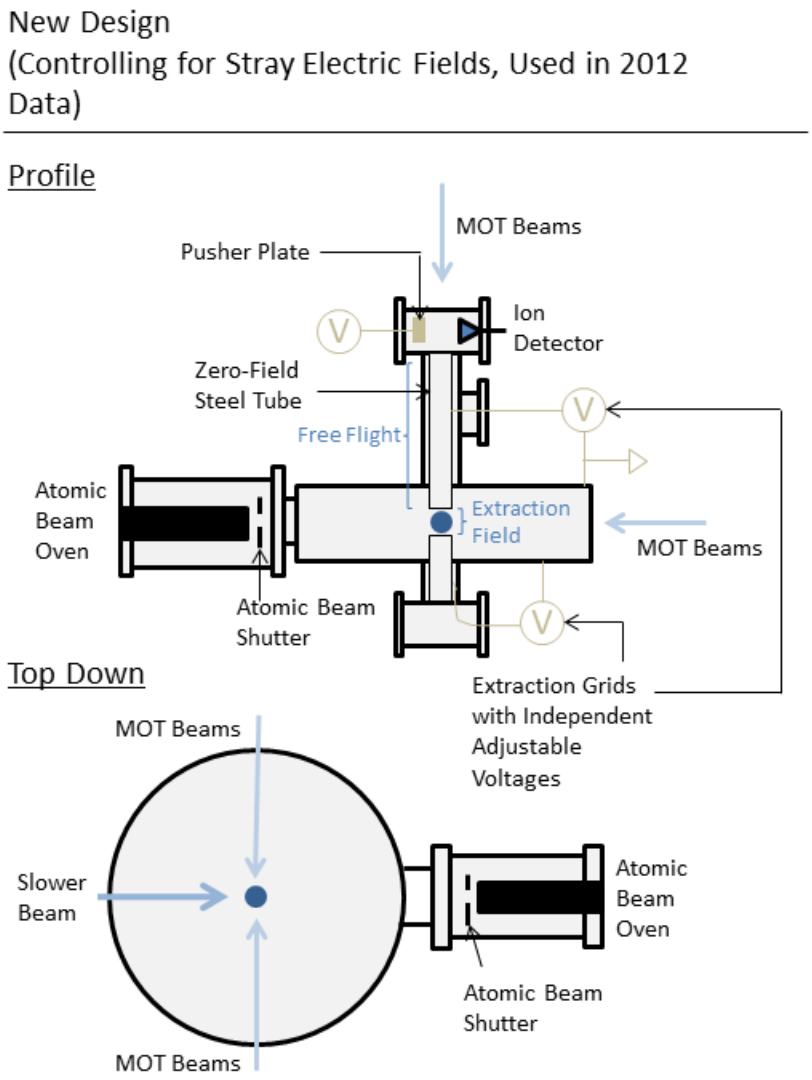

Figure A.2 Altered experimental set-up. The plasma is now extracted vertically between two wide closely spaced grids. The atomic beam oven and shutter have been moved off into a separate anti-chamber, behind a grounded aperture. The plasma moves through a field free region before being repelled by the pushed plate into the ion detector.

The plasma accelerates through the extraction field and then moves into a stainless steel tube at the same voltage as the negative extraction grid. Thus, the plasma spends most of its time of flight in a field free region. During a typical data set it will spend a few hundred nanoseconds in the extraction region and between two and forty microseconds in the field free region. After traveling

through this field free region for $10in$ the plasma encounters a field from a large aluminum "pusher plate." This plate consists of a $1.5in$ diameter $1cm$ block of aluminum hooked up to a power supply. We usually set the power supply for the pusher plate to $200-250V$, depending on the strength of the extraction field and the corresponding velocity of the plasma as it exits the field free region. The pusher plate repels the plasma, pushing it towards the ion detector situated just outside the field free tube.

Since we suspect the primary source of stray fields is the shutter for the atomic beam, we move the entire calcium over-shutter set-up away from the MOT. A $4in$ diameter vacuum chamber to one side houses the atomic beam oven, the shutter and all of the electrical components involved in these devices. A grounded aperture situated at the point where this ante-chamber meets the main chamber makes sure no fields produced in the region distort the fields in the main chamber. A side effect of moving the atomic beam away from the MOT is that fewer atoms reach the MOT region and thus the maximum depth of our MOT is reduced. During the April 2011 data, optical absorption measurements often showed a peak absorption of 60 percent or more with the repump beam. Peak absorption for data with this altered set-up ranges from 20 percent to as low as 14 percent with repump.

A.2.3 Improvements in Signal-to-Noise Ratio

During the alterations described above we also measure the saturation of the ion detector. The ion detector outputs a signal in millivolts. During our original data collection we had assumed that above more than approximately $3mV$ peak voltage the signal would begin to saturate, severely altering the reliability of the signal width and integrated ion signal. We measured look for saturation by changing the sensitivity of the ion detector and recording the ion signal for identical situations. We then divide each signal by its max value and overlay all of them, adjusting for the slight decrease in time of flight that occurs when we increase the ion detector voltage. When there is no

saturation the detector should show identical signals once we perform these adjustments. At the point that the signal begins to saturate the signal will stop lining up with lower voltage signals.

We see no evidence of saturation at as high as $20mV$ peak voltage. This means that for the new data sets we could use the same ion detector sensitivity at all densities while still maintaining good signal to noise ratio. We no longer need to add an adjustment factor to lower density data points.

A.2.4 Data Collection

We collect data on March 15, 20, 27, and 29th, April 5th, and May 3, 10, 17, and 24th of 2012. Between each data set we pause to analyze the data we have collected and make adjustments to improve data. Doing so we realize that there are significant problems with the new set-up and we change our focus each data to overcome these. Ultimately we determine that the problem lies in the expansion model and not in our methods for confirming it and we cease collecting data until we can overcome these issues with the expansion model.

The March and April data is taken by varying the plasma density in a fixed extraction field (time of flight). On May 3, 10, and 17th we experiment with adjusting the offset of the extraction field with respect to the ground of the chamber (see section A.3.2). On May 24, 2012 we experiment with changing the strength of the extraction field and the corresponding time of flight at fixed plasma density.

All data was taken using the same basic method described in section 2.2.1. We record two signals - a probe beam signal from a PMT and a signal from the ion detector - in each of four states corresponding to the open and closed states of shutters on the probe and MOT beams. We average for 64 cycles before recording each signal. During analysis these signals is added, subtracted and divided as described in section 2.3.

A.3 Analysis of New Data

A.3.1 In-Situ Analysis Approach

Rather than collect several weeks worth of data before beginning the analysis process, we perform analysis of each day of data collection before proceeding with the next.

Our original goal is simply to demonstrate that the data we have collected does indeed sweep out the shape of the expansion model, ignoring the specific metrics involved. We ignore the relationship between the probe beam measurement and the integrated ion signal. We also ignore the details of the scaled radius, focusing on the true signal width in μs. We graph integrated ion signal vs. signal width to confirm that the data fits the shape of the model.

A.3.2 Problems with Intrinsic Spread

As we graph the integrated signal vs signal width see that it does not have the shape we expect to see. Figure A.3 shows data taken on April 5, 2012. When varying the density while keeping time of flight constant we expect the signal width to go similarly to the square root of the density (see figure 2.1). In figure A.3 we see a very flat portion at low densities and dramatic increase at the highest measured densities - the exact opposite sort of behavior.

We perform single ion counting of very small signals and discover that there is a minimum width of the signal which does not correspond to the radius of the plasma. A single ion passing through the detector with no ability to expand registers the same signal width as the lowest densities shown in figure A.3 (probably a few thousand ions). We determine that this minimum spread is intrinsic in the ion detector extraction electrodes.

This feature did not seem to exist in the April 2011 data. We initially attribute this spread to the fact that the ion detector is no longer directly in the path produced by the extraction field and that the plasma has to turn the corner under the influence of the pusher plate. This field is not uniform.

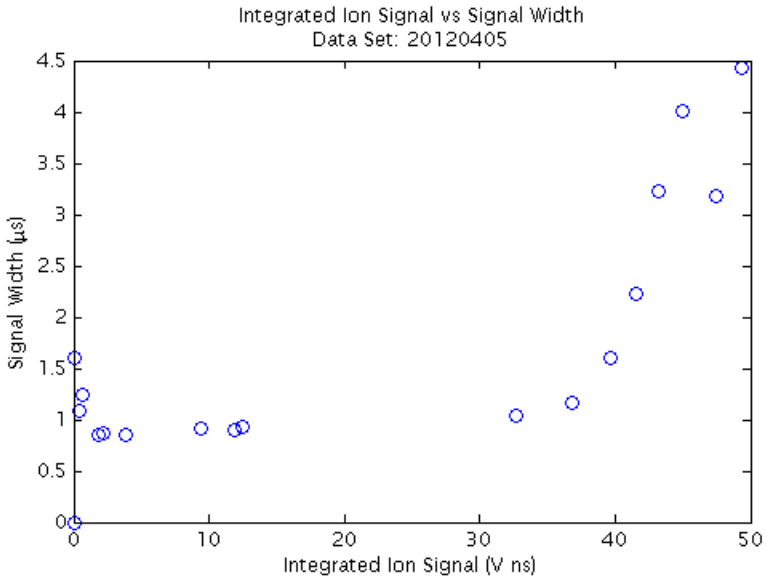

Figure A.3 Integrated ion signal vs signal width at fixed extraction voltage for data taken April 5, 2012. Note that for integrated signals less than $35Vns$ the signal width appears to remain constant around regardless of density. For greater than $35Vns$ the signal begins to increase in something suggestive of the shape predicted by the expansion model.

As such variations in the flight path of the plasma may be exaggerated as the plasma turns the corner causing it to spread out. (See figure A.4)

We note that for this data as well as that used in the March 15, 20, 27 and 29th data the bottom extraction grid is given a positive voltage while the top grid is kept at the ground of the chamber (see figure A.5). While we have done our best to control the field lines in the extraction region, small deviations from linearity are unavoidable. We attempt to correct for this behavior be tracing out the integrated ion signal vs signal width at several different offsets. We apply the same voltage drop of $20V$ across the extraction region but we use four different offsets of that field with respect to the grounded chamber. We hope to see some sort of minimum signal width as we vary the offset. We also hope to lower the width at which the curve "bottoms out."

Figure A.6 shows data taken using the procedure described above. We do not see the behavior expected. Instead we see that the magnitude of the integrated ion signal varies, while the signal

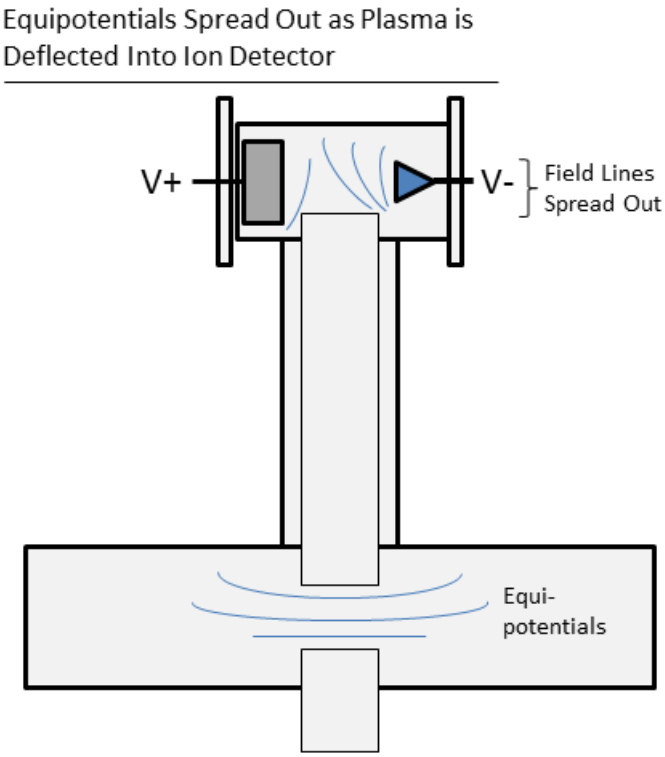

Figure A.4 Diagram showing a likely picture of the field lines and equipotentials of the extraction field. Small deviations from linearity in the extraction field may produce exaggerated results as the plasma is repelled into the ion detector. We attribute the intrinsic minimum width of the ion detector signal to this effect.

width remains consistent. At low densities the signal width varies but this is most likely attributable to lower signal to noise ration in the ion signal. We do see some variation in the width at which the curve flat lines, but in each case it is significant enough to mask the most important features. We conclude that the integrated ion signal is not a reliable relative measure of density.

A.3.3 Varying Time of Flight While keeping Density Constant

Having concluded that the integrated ion signal is not a reliable measure of relative density, we attempt to trace out the curve for fixed density and varying expansion time. Figure A.7 shows time of flight vs signal width at two densities. Overlayed is a third and second polynomial best fit of the

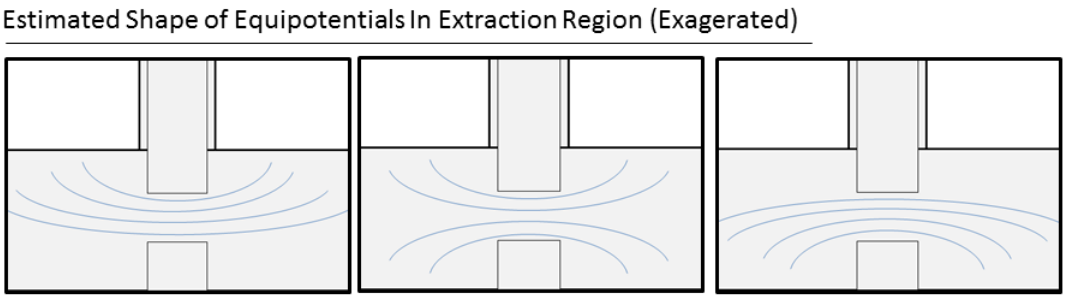

Figure A.5 Exaggerated estimated equipotentials of the plasma with a positive, zero, and negative offset from the ground of the chamber. Note how the shape of the various lines changes as the offset of the extraction voltage changes. This effect should exist even if the relative voltage cross across the grids remains constant.

data, respectively. The expansion model predicts something similar a quadratic expansion as one varies the time of flight (expansion time). This shows just the opposite. The signal width varies as something very close the the square root of the time of flight.

A.4 Conclusion and Outlook

In varying the density at fixed extraction voltage we see the signal change very little at low densities. We initially assume this is a result of the detector. The data shown in figure A.7, however, suggests that at least part of the effect may lie not in the method of data collection but in the model we are trying to confirm. In this data the expansion model suggests that the plasma radius should go as something similar to the square of the expansion time. Instead we see it vary as the square root.

It appears that the description of the plasma given in section 2.1.1, in which Coulomb explosion of the mutually repelling ions causes a self-similar expansion, is not a sufficiently accurate description of what is actually happening within the plasma. If we are to proceed with developing this method, we will need to scrap the current expansion model and take a fundamentally different approach to the derivation.

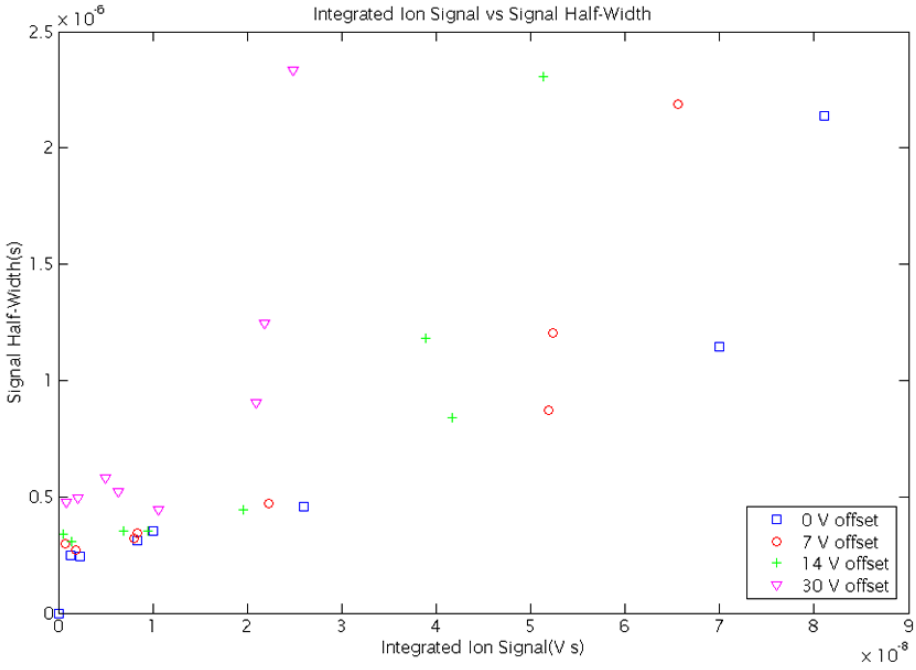

Figure A.6 Integrated ion signal vs signal width for data taken May 3, 2012. We apply the same voltage drop across the extraction region but use four different offsets of this field with respect to the grounded chamber. Note that at high densities the signal width does not vary significantly between extraction field offsets but the integrated ion signal does vary due to these offsets. Also note that at low densities the minimum signal width seems to vary with the delay.

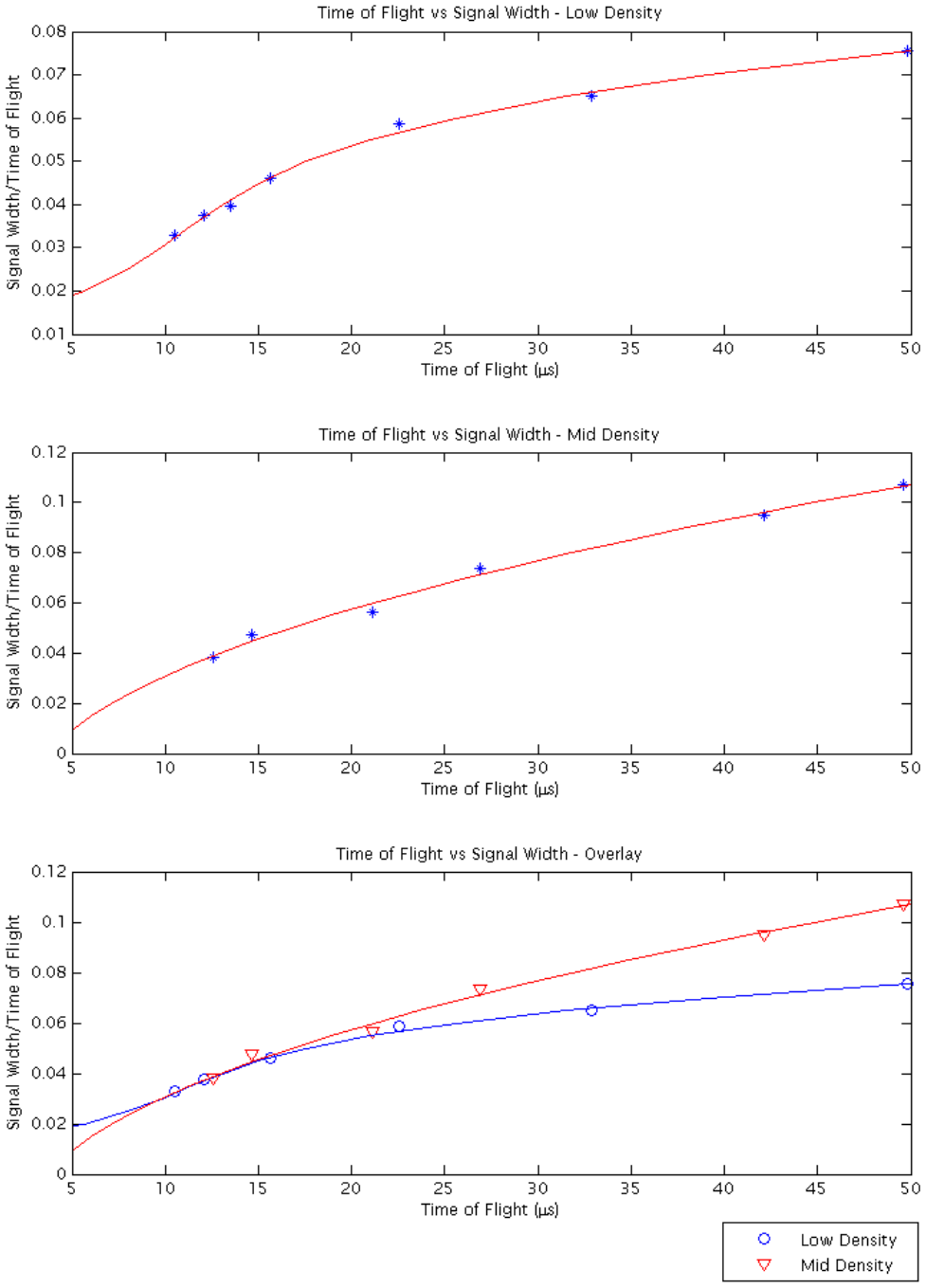

Figure A.7 Time of flight vs signal width at two densities. The signal width varies roughly as the square root of the time of flight.

Bibliography

[1] T. C. Killian and S. L. Rolston, "Ultracold neutral plasmas," Physics Today **63,** 46–51 (2010).

[2] S. D. Bergeson, A. Denning, M. Lyon, and F. Robicheaux, "Density and temperature scaling of disorder-induced heating in ultracold plasmas," Phys. Rev. A **83,** 023409 (2011).

[3] Yukap and Hahn, "Plasma density effects on the three-body recombination rate coefficients," Physics Letters A **231,** 82 – 88 (1997).

[4] T. Killian, Y. Chen, P. Gupta, S. Laha, Y. Martinez, P. Mickelson, S. Nagel, A. Saenz, and C. Simien, "Absoption imagine and spectroscopy of ultracold neutral plamsas," Journal of Physics B: Atomic, Molecular and Optical Physics **38,** S351–S362 (2005).

[5] S. Kulin, T. C. Killian, S. D. Bergeson, and S. L. Rolston, "Plasma Oscillations and Expansion of an Ultracold Neutral Plasma," Phys. Rev. Lett. **85,** 318–321 (2000).

[6] K. A. Twedt and S. L. Rolston, "Electronic Detection of Collective Modes of an Ultracold Plasma," Phys. Rev. Lett. **108,** 065003 (2012).

[7] E. L. Raab, M. Prentiss, A. Cable, S. Chu, and D. E. Pritchard, "Trapping of Neutral Sodium Atoms with Radiation Pressure," Phys. Rev. Lett. **59,** 2631–2634 (1987).

Index